1 **BIOLOGICAL SCIENCES: Developmental Biology; Evolution**

2

3 *Krüppel-like factor* gene function in the ctenophore *Mnemiopsis* suggests an ancient role in 4 promoting cell proliferation in metazoan stem cell niches

5

6 Jason S Presnell[1,2], William E Browne[1,*]

7

8 [1]Department of Biology, University of Miami, Cox Science Center, 1301 Memorial Drive,
9 Miami, FL 33146, USA

10

11 [2]Present Address: Department of Integrative Biology, Oregon State University, 3029 Cordley
12 Hall, Corvallis, OR 97331, USA
13 ORCID ID: 0000-0002-7225-6692

14

15 *Corresponding Author:
16 William E. Browne, Department of Biology, University of Miami, Cox Science Center, 1301
17 Memorial Drive, Miami, FL 33146, USA
18 305-284-3319
19 w.browne@miami.edu
20 ORCID ID: 0000-0001-8200-6489

21

22 Keywords: *Klf*, cell proliferation, stem cell, Ctenophore, *Mnemiopsis leidyi*, morpholino,
23 CRISPR-Cas9

Abstract

All animals possess pluripotent stem cells that during an organism's lifespan give rise to differentiated cell types and are capable of self-renewal. To date studies assessing the function of explicit genes driving the regulation of stem cell renewal and pluripotency have been characterized in bilaterians and a small number of cnidarians. Transcription factor genes critical for regulation of stem cell self-renewal and pluripotency include *Oct4*, *Sox2*, *Klf4, and c-myc* (OSKM) (1–3). In particular, the role of *Klfs* in stem cell renewal and pluripotency has been thoroughly investigated (1, 2, 4–9). In mouse embryonic stem cells the three *Krüppel-like factor* (*Klf*) genes *Klf2*, *Klf4*, and *Klf5* participate in an auto-regulatory activation loop and maintain a transcriptional circuit with *Oct4*, *Sox2*, *c-myc*, and *Nanog* regulating stem cell self-renewal (4). While OSKM gene homologs have been found in the genomes of many metazoans (3, 10, 11), their function is unknown in non-bilaterians. Ctenophora, an ancient non-bilaterian lineage (12–14), possess putative stem cells (11, 15, 16) and have prodigious regenerative capacity (17, 18), making them informative models for investigating the evolution and genetic underpinnings of stem cell maintenance in Metazoa. Ctenophores possess homologs of the OSKM genes (11, 19–21), and while the expression patterns of ctenophore *Sox* paralogs are associated with high rates of cell proliferation in putative stem cell niches (11, 19), little is known about *Pou*, *Klf*, and *c-myc* expression or function. Here we examine the expression of *Klf* homologs in the ctenophore *Mnemiopsis leidyi* and disrupt zygotic *Klf* gene function during embryogenesis using both morpholino oligonucleotides and CRISPR-Cas9. We find that zygotic *MleKlf5a* and *MleKlf5b* play a role in patterning the gastrovascular cavity, pharynx, apical organ, and tentacle bulbs in *M. leidyi*. Simultaneous zygotic knockdown of both *MleKlf5a* and *MleKlf5b* results in the diminution or loss of cell proliferation in endodermal stem cell niches and aberrant endodermal

47 patterning. Our results highlight an ancestral functional role for *Klf* transcription factors in the
48 regulation of rapid cell proliferation in metazoan stem cell niches.
49

50 **Significance**

51 All animals possess pluripotent stem cells that are capable of self-renewal and give rise to
52 differentiated cell types. However studies assessing the function of genes regulating stem cells
53 have been characterized only in bilaterians and cnidarians. *Mnemiopsis leidyi*, a member of the
54 early diverging non-bilaterian phylum Ctenophora, has emerged as an important model system
55 for understanding early animal evolution. *M. leidyi* possess putative stem cell niches in which the
56 expression of 'stemness' genes have been described. Here we characterize the zygotic function
57 of *Krüppel-like factor* (*Klf*) genes during *M. leidyi* embryogenesis. Our results highlight an
58 ancestral role for *Klf* genes in regulating cell proliferation in metazoan endodermal stem cell
59 niches, suggesting very deep conservation of the core transcriptional circuitry critical for stem
60 cell maintenance among extant metazoans.
61

62 **Main**

63 Ctenophores are marine, invertebrate predators characterized by rows of giant cilia fused
64 into 'ctenes' used for locomotion, an aboral and neuronal-rich gravity-sensing (apical) organ, and
65 muscular tentacles lined with sticky colloblast cells used for prey capture (22–27). *M. leidyi*
66 embryos undergo a ctenophore-specific early cleavage program (28, 29), gastrulation takes place
67 ~3-5 hours post fertilization (hpf) followed by tissue organization and organogenesis over the
68 course of the next several hours before hatching as cydippids ~18-22 hpf (30).

69 We used EdU incorporation assays to identify dividing cell populations during
70 embryogenesis. EdU incorporation identified several regions during mid to late embryogenesis
71 with rapid rates of cell proliferation (Fig. 1a-h). Four pairs of ctene rows, one pair in each
72 quadrant, are typically among the first ectodermal structures to form (29). Each ctene plate is
73 made up of polster cells bearing fused giant cilia (31). Beginning at 13 hpf, we observed EdU
74 incorporation in a set of ectodermal cells surrounding each ctene row pair (Fig. 1b, f). In the
75 pharynx, cell proliferation was initially widespread aborally during pharyngeal development and
76 elongation (Fig. 1d). EdU incorporation in the pharynx subsequently becomes spatially restricted
77 to two domains, one orally near the stomodeal opening, and the other aborally that includes the
78 pharyngeal region forming the junction with the gastrovascular cavity (Fig. 1h). In the apical
79 organ, cell proliferation was localized to the developing polar fields and a small subset of cells
80 located deep within the epithelial floor along tentacular axis (Fig. 1a, e). Due to their proximity
81 to where new lithocytes are formed, these deeper proliferative cells likely represent lithocyte
82 progenitor cells (32).
83 Flanking the apical organ along the tentacular axis, ectodermal invaginations and internal
84 medial endodermal cell bands form the tentacle bulb organ (33–35) contributing to both the
85 ectodermal tentacular lateral ridges and the endodermal tentacular median ridges respectively,
86 each harboring progenitor cells that give rise to colloblasts and tentacle muscle (33–35). During
87 tentacle bulb development EdU incorporation was initially observed in the median ridges (Fig.
88 1c-d). Later EdU incorporation was detected along the length of the median ridges and in the
89 lateral ridges (Fig. 1g-h). An Edu pulse followed by a 24-hour chase revealed that these
90 proliferative cells gave rise preferentially to tentacular muscle cells (S1). Previous cell
91 proliferation studies in another ctenophore species, *Pleurobrachia pileus*, identified gene

92 expression indicative of 'stemness' such as *Piwi*, *Vasa*, *Nanos*, and *Sox* coincident with EdU-
93 positive cells in proliferative stem cell niches (15, 19) similar to those observed during *M. leidyi*
94 embryogenesis.

95 The genome of *M. leidyi* contains three *Klf* genes: *MleKlf5a*, *MleKlf5b*, and *MleKlfX*
96 (20). *MleKlf5a* and *MleKlf5b* are the result of a lineage-specific duplication within the
97 Ctenophora. *MleKlfX* is highly derived with no clear orthology to any known metazoan *Klf* clade.
98 *MleKlf5a* and *MleKlf5b* transcripts are maternally loaded (21) and transcripts are detected in all
99 embryonic cells through gastrulation (Fig. 1i-l). Maternal loading has been observed in a number
100 of *Klf* genes among bilaterians (36–38). Following gastrulation, *MleKlf5a* and *MleKlf5b* zygotic
101 expression is spatially localized to regions undergoing high rates of cell proliferation coincident
102 with EdU incorporation (Fig1 a-h, m-x). *MleKlf5a* and *MleKlf5b* expression overlap extensively
103 in endodermal domains during embryonic development (Fig. 1m-x). Interestingly a single
104 ectodermal expression domain unique to *MleKlf5b* is detected in proliferative cells flanking
105 developing ctene row polster cells (Fig. 1b, f, S2a, b).

106 Within the pharynx, *MleKlf5a* and *MleKlf5b* expression is confined to the interior-most
107 cell layer. Expression in the aboral-most portion of the pharynx is associated with cells that form
108 the junction with the central gastrovascular cavity (infundibulum) and also throughout the
109 endodermal epithelia lining the developing infundibulum (Fig. 1n, p, r, t, v, x). During the initial
110 formation of the aboral apical organ, *MleKlf5a* and *MleKlf5b* expression is detected in the apical
111 organ floor epithelia. *MleKlf5a* and *MleKlf5b* expression in the apical organ becomes
112 progressively restricted to cells that positionally correlate with putative lithocyte progenitor cells
113 (Fig. 1r, t, v, x). Within the developing tentacle bulbs, expression patterns of *MleKlf5a* and
114 *MleKlf5b* mirror EdU incorporation in regions of rapid cell proliferation (Fig. 1c-e, g-h, m-x).

115 *MleKlf5a* and *MleKlf5b* are highly expressed in the median ridge of developing tentacle bulbs
116 (Fig. 1m-x), suggesting that *MleKlf5a* and *MleKlf5b* may play a role in the maintenance of the
117 median ridge tentacular stem cell niche. In summary, *MleKlf5a* and *MleKlf5b* paralog expression
118 extensively overlaps in embryonic domains with high rates of cell proliferation. These regions
119 are known to express additional genes associated with stemness such as *Piwi*, *Vasa*, *Nanos*, and
120 *Sox* (11, 15, 16, 19). *MleKlf5a* and *MleKlf5b* expression identifies putative stem cell niches
121 within the aboral region of the pharynx, coincides with putative lithocyte progenitor cells located
122 in epithelial floor of the apical organ and progenitor cells located in the median ridge of the
123 tentacle bulb.

124 In contrast to *MleKlf5a* and *MleKlf5b* expression patterns, *MleKlfX* expression is
125 restricted to late stage embryos, first appearing ~16 hpf and does not appear to be associated with
126 EdU-positive cells (S2c, d). *MleKlfX* expression is restricted to a small number of cells within
127 the apical organ. A set of *MleKlfX* expressing cells are located centrally, deep within the
128 epithelial floor of the developing apical organ. A second shallower set is located in each quadrant
129 of the developing apical organ, just medial of the ciliated grooves. Two cell clusters located
130 along the tentacular plane are perpendicular to two additional cell clusters, forming a cross-
131 shaped pattern. These *MleKlfX* expressing cells correspond with the position of apical organ
132 lamellate bodies, putative photoreceptor cells (39, 40), suggesting that *MleKlfX* may play a role
133 in the differentiation of light sensitive neuronal cell types in the apical organ. In summary,
134 *MleKlfX* a highly divergent gene in *M. leidyi*, appears to be expressed in a set of differentiated
135 neuronal cells, possibly involved with light sensing.

136 To characterize zygotic *Klf* gene function in *M. leidyi,* we used both splice-blocking
137 morpholinos (sbMOs) and CRISPR-Cas9 genome editing to abrogate gene function during

138 embryonic development (Fig. 2). Knockdown of *MleKlfX* failed to produce any obvious
139 morphological phenotypes, so we focus here on the *MleKlf5a* and *MleKlf5b* results. It has been
140 shown that co-expressed KLFs bind to shared downstream regulatory targets resulting in
141 complex functional outcomes. For example, KLF2, KLF4, and KLF5 have redundant roles in the
142 downstream regulation of *Nanog* (4), whereas competition between KLF1 and KLF3 for binding
143 sites can result in differential functional outcomes (41). For this reason we sought to maximize
144 the efficiency of generating an observable phenotype by performing simultaneous *MleKlf5a* and
145 *MleKlf5b* knockdown with both sbMO and CRISPR-Cas9 genome editing experiments. We
146 injected single-cell embryos with either *MleKlf5a*+*MleKlf5b* sbMOs or *MleKlf5a-*
147 *sgRNA*+*MleKlf5b-sgRNA*. Microinjected embryos were incubated to ~20 hpf and live stained
148 with vital dyes (Fig. 3). Morphant and crispant specimens were live imaged and compared to
149 equivalent late stage wildtype embryos from the same spawning events. A selection of
150 morphants and crispants were then subjected to single embryo RNA or DNA extractions
151 respectively for gene knockdown validation. Two sbMOs were designed for each gene (Fig. 2a,
152 e). These produced splice-blocking errors in morphants through exon skipping and/or intron
153 retention (Fig. 2b, f). An initial set of 4 sgRNAs were designed for *MleKlf5a* and *MleKlf5b*
154 (Table 1) based on the *M. leidyi* reference genome (42, 43). A single sgRNA for each gene,
155 *MleKlf5a-sgRNA4* and *MleKlf5b-sgRNA3* (Fig. 2a, e), proved efficient at mediating Cas9 double-
156 stranded break activity at the target loci (Fig. 2c-d, g-h). Sanger sequencing followed by ICE
157 analysis revealed clear degradation of signal in the crispants at the target loci compared to
158 control embryos (Fig. 2c, g), indicating *MleKlf5a-sgRNA4* and *MleKlf5b-sgRNA3* targeted Cas9
159 exonuclease activity produced indels and frameshift mutations (S3b). Control injections with a
160 standard control MO, Cas9 protein alone, and sgRNAs alone had no detectable effect on

161 embryonic development (S3a). No evidence of off-target Cas9 activity was observed in tested
162 loci (Table 2) thus phenotypes generated via both double gene abrogation approaches in our
163 study were due to the disruption of *MleKlf5a* and *MleKlf5b* activity.

164 Both *MleKlf5a+MleKlf5b* morphants and crispants generated an allelic series of
165 phenotypes (Fig. 3a-p). While morphants and crispants phenocopied one another, a higher
166 proportion of severe phenotypes were observed among crispants as compared to morphants as
167 expected (Fig. 3s), reflecting the effects of Cas9 mediated genome editing versus titration of
168 functional mRNAs by sbMOs. In contrast to the observation of primarily severe phenotypes in
169 the crispant *MleKlf5a-sgRNA4+MleKlf5b-sgRNA3* double gene knockdowns (Fig. 3o-p; Fig. 4e-
170 f, l-m), single gene knockdown with either *MleKlf5a-sgRNA4* or *MleKlf5b-sgRNA3* generated
171 predominantly mild phenotypes (S4). This suggests that *MleKlf5a* and *MleKlf5b* likely have
172 functionally redundant regulatory roles in maintaining proliferative endodermal stem cell niches
173 during embryonic development. Further investigation will be needed to determine whether
174 *MleKlf5a* and *MleKlf5b* are acting on the same direct downstream targets or acting indirectly on
175 complementary non-overlapping sets of genes regulating cell proliferation. For example, in
176 mouse embryonic stem cells, pluripotency and proliferation are maintained through differential
177 inhibition of endoderm and mesoderm by *Klf4* and *Klf5* respectively (44).

178 Ctenes are initially established by maternal factors (29), new polster cells and ctene row
179 expansion begin post-hatching at the cydippid stage (45). With regard to the unique ectodermal
180 expression domain of *MleKlf5b*, no ectodermal or individual ctene patterning phenotype was
181 observed in *MleKlf5b-sgRNA3* or *MleKlf5a-sgRNA4* crispants nor double gene abrogation
182 experiments. However, rows of ctenes showed some disorganization in phenotypically severe
183 morphants and crispants, possibly reflecting extended regions of close contact between ectoderm

184 and underlying endoderm (Fig. 3g, o). Notably, in phenotypically mild morphants and crispants,
185 ctene development did not occur in 'quadrants' in which endoderm did not make close contact
186 with ectoderm (Fig. 3e, m). This result further corroborates prior analyses indicating that ctene
187 development is associated with inductive interactions between endodermal and ectodermal cell
188 lineages (46, 47). Thus the observed EdU- and *MleKlf5b*-positive ectodermal cells (Fig. 1b, f:
189 S2a-b) likely contribute to ctene row expansion post-hatching and/or perhaps also play a role in
190 the growth and maintenance of surrounding ectodermal epithelia post-hatching.

191 Embryos with mild phenotypes underwent pharyngeal elongation concomitant with
192 mesogleal deposition and an increase in size; however, they displayed disorganized endodermal
193 patterning associated with the aboral end of the pharynx and infundibular gastrovascular cavity
194 (Fig. 3e-f, m-n). In some cases we observed instances of pharyngeal bifurcation at the junction
195 with the gastrovascular cavity (Fig. 3f, n; S4b; S5). In contrast, embryos classified as having
196 severe phenotypes (Fig. 3g-h, o-p) failed to increase in size, likely reflecting a lack of ECM
197 extrusion into the mesogleal space, resulting in internal embryonic spaces being
198 disproportionately occupied by gastrovascular endoderm and a failure of normal pharyngeal
199 elongation. Assessment of cell proliferation in *MleKlf5a-sgRNA4+MleKlf5b-sgRNA3* crispants
200 revealed a dramatic reduction of EdU incorporation at the aboral end of the pharynx (Fig. 3q, r).
201 These results suggest that zygotic *MleKlf5a* and *MleKlf5b* play a coordinated role in the growth
202 and patterning of the gastrovascular cavity and pharynx, including the aboral region of the
203 pharynx that develops pharyngeal folds and the pharyngeal gastrovascular junction that contains
204 the ciliary mill (48), presumably through maintenance of cell proliferation in putative
205 endodermal stem cell niches in these tissues.

206 Across both morphants and crispants, additional patterning defects were observed in the
207 apical organ epithelial floor (Fig. 3; Fig. 4). *MleKlf5a* and *MleKlf5b* knockdown resulted in a
208 significant reduction of apical organ lithocytes as compared to control embryos (Fig. 4a-g). By
209 20 hpf, control embryo statocysts contain ~7 lithocytes (Fig. 4a-b, g). *MleKlf5a+MleKlf5b*
210 morphants had an average ~4 lithocytes (Fig. 4g), with three lacking lithocytes entirely (Fig. 4c,
211 d). *MleKlf5a-sgRNA4+MleKlf5b-sgRNA3* crispants had an average of ~2 lithocytes (Fig. 4g),
212 with five completely lacking lithocytes (Fig. 4e, f). In embryos lacking lithocytes, both balancer
213 cilia and dome cilia were present (Fig. 4d, f), reflecting that lithocytes are derived from
214 endoderm while the balancer and dome cilia are derived from ectoderm (34). This suggests that
215 *MleKlf5a* and *MleKlf5b* play a role in maintenance of endodermally-derived lithocyte progenitor
216 cells in the apical organ.
217 Simultaneous abrogation of *MleKlf5a* and *MleKlf5b* also resulted in a dramatic reduction
218 in tentacle bulb size, particularly notable in the tentacular median ridge (Fig. 3; Fig. 4h-n). We
219 measured the length of the tentacular median ridge and found significant differences between
220 control and injected embryos (Fig. 4n; S6). In control embryos the tentacular median ridge was,
221 on average, 23 µm in length, whereas in *MleKlf5a+MleKlf5b* morphants and *MleKlf5a-*
222 *sgRNA4+MleKlf5b-sgRNA3* crispants, the average tentacular median ridge length was ~18 µm
223 and ~9 µm respectively (Fig. 4n). Furthermore, we observed that 15% of the *MleKlf5a+MleKlf5b*
224 morphants and 29% of the *MleKlf5a-sgRNA4+MleKlf5b-sgRNA3* crispants lacked tentacular
225 median ridges altogether (Fig. 4j-m). Assessment of cell proliferation in *MleKlf5a-*
226 *sgRNA4+MleKlf5b-sgRNA3* crispants revealed a dramatic reduction in EdU incorporation in the
227 tentacular median ridges, but not in the tentacular lateral ridges (Fig. 3q, r). This indicates that
228 proliferation in the tentacular lateral ridge stem cell niches was largely unaffected in both

229 morphants and crispants. Lateral ridge stem cells give rise to tentacle epithelia and colloblasts
230 (15, 35), which were present in embryos with reduced median ridges (Fig. 4j-m). Our results
231 support a requirement for *MleKlf5a* and *MleKlf5b* activity for normal tentacle bulb development
232 and specifically for production of tentacle root muscle through maintenance of cell proliferation
233 in the endodermally-derived tentacular median ridge stem cell niche.

234 In this study, we used both sbMOs and Cas9-mediated genome editing to coordinately
235 abrogate zygotic *MleKlf5a* and *MleKlf5b* gene function during *M. leidyi* embryonic development.
236 We show that Cas9-mediated genome editing is an effective method for performing
237 combinatorial gene function assays in F0 ctenophore embryos. Along with recent RNA-seq data
238 highlighting candidate genes associated with zygotic gene activation and specific cell types in
239 ctenophores (21, 35, 49), sbMO and CRISPR-Cas9 based gene function assays in *M. leidyi* will
240 provide much needed insight into the genetic underpinnings of ctenophore biology and further
241 our understanding of early metazoan evolution. Our results highlight an essential role for zygotic
242 *MleKlf5a* and *MleKlf5b* activity in promoting cell proliferation in tissue and organ specific stem
243 cell niches that remain active throughout the lifespan of *M. leidyi* that produce a number of
244 terminally differentiated cell types unique to the Ctenophora. Our results further suggest that the
245 functional activity of *Klfs* in promoting cell proliferation within stem cell niches represents a
246 conserved ancestral function of this gene family across the Metazoa.
247

248 **Methods**

249 **Cloning and *in situ* hybridization**

250 RNA was extracted using Trizol (Thermo Fisher Scientific) from *Mnemiopsis* embryos
251 collected at different stages of development and used to generate cDNA libraries (SMARTer kit,

252 Clontech). The coding sequences of *MleKlf5a*, *MleKlf5b*, and *MleKlfX* were amplified from
253 cDNA (Table 1) and cloned into pGEM-T Easy vector (Promega). The cloned fragments were
254 used as templates for *in vitro* transcription (MEGAscript, Ambion) of antisense digoxigenin-
255 labeled (Digoxigenin-11-UTP, Roche) riboprobes.

256 *In situ* hybridization followed (50). Riboprobes were used at a final concentration of ~0.5
257 ng/µl and hybridized with embryos for 24 hours. After color development, nuclei were labeled
258 with either DAPI (Molecular Probes) or Hoechst 33342 (Molecular Probes) in 1x PBS. Embryos
259 were immediately imaged or stored at -20°C in 70% glycerol in 1x PBS. Images were acquired
260 using a Zeiss Axio Imager.Z2, Zeiss AxioCam MRm Rev3 camera, and Zeiss Zen Blue software.
261 Fluorescent Z-stacks were deconvolved, post-processed for brightness and contrast and
262 assembled in Adobe Photoshop. Monochrome brightfield images were inverted, pseudocolored,
263 and overlaid onto fluorescent images of labeled nuclei. Samples were stored at -20°C in 70%
264 glycerol in 1x PBS.

265

266 **Vital Dye staining**

267 Live embryos were incubated in filtered seawater (FSW) containing a final concentration
268 of 100 nM MitoTracker (Deep Red FM, Molecular Probes), 100 nM LysoTracker (Red DND-99,
269 Molecular Probes), and 10 ng/µl Hoechst 33342 for one hour at room temperature. Live embryos
270 were then placed on glass microscope slides in a drop of FSW and relaxed with a drop of 6.5%
271 $MgCl_2$ (in dH_2O) on a coverslip positioned with clay feet. Images were acquired using a Zeiss
272 Axio Imager.Z2, Zeiss AxioCam MRm Rev3 camera, and Zeiss Zen Blue software. Fluorescent
273 Z-stacks were deconvolved, post-processed for brightness and contrast, and assembled in Adobe
274 Photoshop.

275

276 **EdU labeling**

277 Click-iT® EdU Alexa Fluor® 647 Imaging Kit (ThermoFisher Scientific) was used for
278 identification of proliferating cells. Embryos were collected at different developmental stages
279 and pulse incubated for 25 minutes with 100 µM EdU in a solution of a 1:1 volumetric ratio of
280 FSW to 6.5% $MgCl_2$ (dissolved in dH_2O) at room temperature. The EdU solution was washed
281 out and embryos were either fixed immediately or allowed to continue to develop during a 24-
282 hour chase and subsequently fixed. Embryos were fixed with 4% PFA in FSW for 30 minutes at
283 room temperature, washed with 3% BSA in 1x PBS, and incubated with 0.5% Triton X-100 in
284 1x PBS for 20 minutes at room temperature. Fixed embryos were washed with 3% BSA in 1x
285 PBS and stored at 4°C until used for EdU detection as per manufacturer protocol. Embryos were
286 subsequently washed with 1x PBS and mounted on glass microscope slides. Images were
287 acquired using a Zeiss Axio Imager.Z2, Zeiss AxioCam MRm Rev3 camera, and Zeiss Zen Blue
288 software. Fluorescent Z-stacks were deconvolved, post-processed for brightness and contrast,
289 and assembled in Adobe Photoshop or FIJI (51).

290

291 **Microinjection**

292 Laboratory cultures of adult *Mnemiopsis leidyi* on a ~12 hr:12 hr light:dark cycle were
293 spawned ~4 hours post darkness (hpd). At ~3.5 hpd individual adult *M. leidyi* were placed into 8-
294 inch glass bowls and screened for mature sperm and eggs. Freshly fertilized eggs were collected
295 by pipette.

296 Microinjection needles were pulled with a Brown micropipette puller (P-1000, Sutter
297 Instrument Company) using aluminosilicate glass capillaries (AF100-64-10, Sutter Instrument

298 Company). Pulled capillaries were beveled using a microelectrode beveler (BV-10, Sutter
299 Instrument Company). Beveled capillary needles were loaded via backfilling with injection
300 cocktails mixed with fluorescently-conjugated dextran (Invitrogen) (used to assess injection
301 success). Loaded capillary needles were mounted to a Xenoworks microinjection system (Sutter
302 Instrument Company) paired to a Zeiss Discovery V8 epiflourescent stereomicroscope.
303 Fertilized *M. leidyi* eggs were collected and passed sequentially through a 500 µm and a
304 400 µm cell strainer (pluriSelect Life Science) to remove excess mucus and egg jelly. Embryos
305 were then washed with 1x Penicillin/Streptomycin:FSW (PS:FSW). The embryonic vitelline
306 membranes were removed in gelatin coated dishes with acid-sharpened tungsten needles.
307 Embryos were then carefully transferred to an injection dish. After microinjection, embryos were
308 kept at room temperature until reaching the desired development stage for further analyses.
309 To determine if removing the vitelline membrane had an effect on embryogenesis, we
310 scored the percentage of normal development in embryos that were removed from the vitelline
311 membrane but not injected. There was no significant difference in the percentage of normal
312 development between embryos kept in their vitelline membrane (85%, n=161) and those that
313 were devitellinized but uninjected (80%, n=217; χ^2=1.5272, p=0.217; Extended Data Fig. 3a).
314

315 **Morpholino oligonucleotides**

316 Splice-blocking morpholino oligonucleotides (sbMOs, Gene Tools) were designed for
317 both *MleKlf5a* (*ML00922a*) and *MleKlf5b* (*ML25776a*). *MleKlf5a* sbMO #1 and sbMO #2
318 targeted intron 2-exon 3 and intron 3-exon 4 boundaries, respectively. *MleKlf5b* sbMO #1 and
319 sbMO #2 targeted exon 6-intron 6 and exon 7-intron 7 boundaries, respectively. A standard
320 control MO was used as a negative control. Sequences of sbMOs are listed in Table 1. Stock

321 solutions of sbMO in dH_2O were stored at room temperature. sbMO injection cocktail solutions
322 consisted of a final sbMO concentration of ~333 nM and ~0.5 mg/ml fluorescent dextran
323 (rhodamine or Alexa-Fluor 488, 10,000 MW, Invitrogen) in 35% glycerol. After phenotypic
324 analyses RNA was extracted from individual embryos (Arcturus PicoPure, ThermoFisher) and
325 cDNA prepared. Gene-specific primers were used on cDNA (OneTaq One-Step RT-PCR, New
326 England Biolabs) to evaluate aberrant transcript splicing via gel electrophoresis.
327

328 **CRISPR-Cas9**

329 We followed a cloning-free method to generate sgRNAs (43, 52). PCR amplified
330 templates were generated by annealing a 20-nt universal tracrRNA oligo to a sgRNA-specific
331 oligo that consisted of a T7 promoter, followed by the sgRNA target sequence, and a
332 complementary sequence to the tracrRNA oligo (Table 1). These templates were then *in vitro*
333 transcribed (MEGAscript, Ambion) to generate sgRNAs. The CasOT program (53) and *M. leidyi*
334 reference genome (42) were used to identify sgRNA target sites for *MleKlf5a* (*ML00922a*),
335 *MleKlf5b* (*ML25776a*), and *MleKlfX* (*ML20061a*). We selected sgRNAs that had no fewer than
336 four mismatches to alternative genomic sites to minimize potential off-target site (OTS) activity
337 (Table 1). Recombinant Cas9 protein (PNA Bio) and sgRNAs were injected at concentrations of
338 400 ng/µl of Cas9 protein and 100 ng/µl for each sgRNA. After phenotypic analysis, genomic
339 DNA was extracted from individual embryos (QIAamp DNA Micro, Qiagen) and each sgRNA
340 target site was amplified and Sanger sequenced. The ICE analysis tool (Synthego,
341 https://ice.synthego.com/#/) was used to determine Cas9 efficiency for each sgRNA. ICE
342 analysis gives two scores: an ICE score which reflects the percentage of indels found and a KO
343 score which reflects the percentage of indels that produce a frameshift mutation.

344

345 **References**

346 1. Takahashi K, Yamanaka S (2006) Induction of pluripotent stem cells from mouse
347 embryonic and adult fibroblast cultures by defined factors. *Cell* 126(4):663–676.
348 2. Takahashi K, et al. (2007) Induction of pluripotent stem cells from adult human fibroblasts
349 by defined factors. *Cell* 131(5):861–872.
350 3. Rosselló RA, et al. (2013) Mammalian genes induce partially reprogrammed pluripotent
351 stem cells in non-mammalian vertebrate and invertebrate species. *eLIFE* 2:e00036.
352 4. Jiang J, et al. (2008) A core Klf circuitry regulates self-renewal of embryonic stem cells. *Nat*
353 *Cell Biol* 10(3):353–360.
354 5. Parisi S, et al. (2010) Direct targets of Klf5 transcription factor contribute to the
355 maintenance of mouse embryonic stem cell undifferentiated state. *BMC Biol* 8:128.
356 6. McConnell BB, Yang VW (2010) Mammalian Krüppel-like factors in health and diseases.
357 *Physiol Rev* 90(4):1337–1381.
358 7. Parisi S, et al. (2008) Klf5 is involved in self-renewal of mouse embryonic stem cells. *J Cell*
359 *Sci* 121(Pt 16):2629–2634.
360 8. Nandan MO, Yang VW (2009) The role of Krüppel-like factors in the reprogramming of
361 somatic cells to induced pluripotent stem cells. *Histol Histopathol* 24(10):1343–1355.
362 9. Nandan MO, Ghaleb AM, Bialkowska AB, Yang VW (2015) Krüppel-like factor 5 is
363 essential for proliferation and survival of mouse intestinal epithelial stem cells. *Stem Cell*
364 *Res* 14(1):10–19.
365 10. Steele RE, David CN, Technau U (2011) A genomic view of 500 million years of cnidarian
366 evolution. *Trends Genet* 27(1):7–13.

367 11. Schnitzler CE, Simmons DK, Pang K, Martindale MQ, Baxevanis AD (2014) Expression of
368 multiple *Sox* genes through embryonic development in the ctenophore *Mnemiopsis leidyi* is
369 spatially restricted to zones of cell proliferation. *Evodevo* 5:15.
370 12. Dunn CW, et al. (2008) Broad phylogenomic sampling improves resolution of the animal
371 tree of life. *Nature* 452(7188):745–749.
372 13. Hejnol A, et al. (2009) Assessing the root of bilaterian animals with scalable phylogenomic
373 methods. *Proc Biol Sci* 276(1677):4261–4270.
374 14. Whelan NV, et al. (2017) Ctenophore relationships and their placement as the sister group to
375 all other animals. *Nat Ecol Evol*. doi:10.1038/s41559-017-0331-3.
376 15. Alié A, et al. (2011) Somatic stem cells express *Piwi* and *Vasa* genes in an adult ctenophore:
377 Ancient association of "germline genes" with stemness. *Dev Biol* 350(1):183–197.
378 16. Reitzel AM, Pang K, Martindale MQ (2016) Developmental expression of "germline"- and
379 "sex determination"-related genes in the ctenophore *Mnemiopsis leidyi*. *Evodevo* 7:17.
380 17. Martindale MQ (1986) The ontogeny and maintenance of adult symmetry properties in the
381 ctenophore, *Mnemiopsis mccradyi*. *Dev Biol* 118(2):556–576.
382 18. Martindale MQ (2016) The onset of regenerative properties in ctenophores. *Curr Opin*
383 *Genet Dev* 40:113–119.
384 19. Jager M, Quéinnec E, Chiori R, Le Guyader H, Manuel M (2008) Insights into the early
385 evolution of SOX genes from expression analyses in a ctenophore. *J Exp Zool B Mol Dev*
386 *Evol* 310(8):650–667.
387 20. Presnell JS, Schnitzler CE, Browne WE (2015) KLF/SP Transcription Factor Family
388 Evolution: Expansion, Diversification, and Innovation in Eukaryotes. *Genome Biol Evol*
389 7(8):2289–2309.

390 21. Davidson PL, et al. (2017) The maternal-zygotic transition and zygotic activation of the
391 *Mnemiopsis leidyi* genome occurs within the first three cleavage cycles. *Mol Reprod Dev*.
392 doi:10.1002/mrd.22926.
393 22. Chun C (1880) *Die ctenophoren des Golfes von Neapel und der angrenzenden meeres-*
394 *abschnitte* (W. Engelmann, Leipzig).
395 23. von Byern J, Mills CE, Flammang P (2010) Bonding tactics in ctenophores—morphology
396 and function of the colloblast system. *Biological Adhesive Systems: From Nature to*
397 *Technical and Medical Application*, eds von Byern J, Grunwald I (Springer, Vienna), pp 29–
398 40.
399 24. Ryan JF, et al. (2013) The genome of the ctenophore *Mnemiopsis leidyi* and its implications
400 for cell type evolution. *Science* 342(6164):1242592.
401 25. Moroz LL, et al. (2014) The ctenophore genome and the evolutionary origins of neural
402 systems. *Nature* 510(7503):109–114.
403 26. Tamm SL (2014) Cilia and the life of ctenophores. *Invertebr Biol* 133(1):1–46.
404 27. Pang K, Martindale MQ (2008) Ctenophores. *Curr Biol* 18(24):R1119–20.
405 28. Freeman G (1976) The effects of altering the position of cleavage planes on the process of
406 localization of developmental potential in ctenophores. *Dev Biol* 51(2):332–337.
407 29. Fischer AH, Pang K, Henry JQ, Martindale MQ (2014) A cleavage clock regulates features
408 of lineage-specific differentiation in the development of a basal branching metazoan, the
409 ctenophore *Mnemiopsis leidyi*. *Evodevo* 5(1):4.
410 30. Pang K, Martindale MQ (2008) Comb Jellies (Ctenophora): A Model for Basal Metazoan
411 Evolution and Development. *CSH Protoc* 2008:db.emo106.
412 31. Tamm SL (1973) Mechanisms of Ciliary Co-Ordination in Ctenophores. *J Exp Biol*

413 59(1):231–245.

414 32. Tamm SL (2014) Formation of the statolith in the ctenophore *Mnemiopsis leidyi*. *Biol Bull*
415 227(1):7–18.

416 33. Martindale MQ, Henry JJ (1997) Experimental Analysis of Tentacle Formation in the
417 Ctenophore *Mnemiopsis leidyi*. *Biol Bull* 193(2):245–247.

418 34. Martindale MQ, Henry JQ (1999) Intracellular fate mapping in a basal metazoan, the
419 ctenophore *Mnemiopsis leidyi*, reveals the origins of mesoderm and the existence of
420 indeterminate cell lineages. *Dev Biol* 214(2):243–257.

421 35. Babonis LS, et al. (2018) Integrating embryonic development and evolutionary history to
422 characterize tentacle-specific cell types in a ctenophore. *Mol Biol Evol*.
423 doi:10.1093/molbev/msy171.

424 36. De Graeve F, et al. (2003) Identification of the *Drosophila* progenitor of mammalian
425 Krüppel-like factors 6 and 7 and a determinant of fly development. *Gene* 314:55–62.

426 37. Weber U, Rodriguez E, Martignetti J, Mlodzik M (2014) Luna, a Drosophila KLF6/KLF7, is
427 maternally required for synchronized nuclear and centrosome cycles in the preblastoderm
428 embryo. *PLoS One* 9(6):e96933.

429 38. Blakeley P, et al. (2015) Defining the three cell lineages of the human blastocyst by single-
430 cell RNA-seq. *Development* 142(20):3613.

431 39. Horridge GA (1964) Presumed photoreceptive cilia in a ctenophore. *Quart J Micr Sci*
432 105:311–317.

433 40. Schnitzler CE, et al. (2012) Genomic organization, evolution, and expression of
434 photoprotein and opsin genes in *Mnemiopsis leidyi*: a new view of ctenophore photocytes.
435 *BMC Biol* 10:107.

436 41. Ilsley MD, et al. (2017) Krüppel-like factors compete for promoters and enhancers to fine-
437 tune transcription. *Nucleic Acids Res* 45(11):6572–6588.
438 42. Moreland RT, et al. (2014) A customized Web portal for the genome of the ctenophore
439 *Mnemiopsis leidyi*. *BMC Genomics* 15:316.
440 43. Varshney GK, et al. (2015) High-throughput gene targeting and phenotyping in zebrafish
441 using CRISPR/Cas9. *Genome Res* 25(7):1030–1042.
442 44. Aksoy I, et al. (2014) Klf4 and Klf5 differentially inhibit mesoderm and endoderm
443 differentiation in embryonic stem cells. *Nat Commun* 5:3719.
444 45. Tamm SL (2012) Patterns of comb row development in young and adult stages of the
445 ctenophores *Mnemiopsis leidyi* and *Pleurobrachia pileus*. *J Morphol* 273(9):1050–1063.
446 46. Henry JQ, Martindale MQ (2001) Multiple inductive signals are involved in the
447 development of the ctenophore *Mnemiopsis leidyi*. *Dev Biol* 238(1):40–46.
448 47. Henry JQ, Martindale MQ (2004) Inductive interactions and embryonic equivalence groups
449 in a basal metazoan, the ctenophore *Mnemiopsis leidyi*. *Evol Dev* 6(1):17–24.
450 48. Presnell JS, et al. (2016) The Presence of a Functionally Tripartite Through-Gut in
451 Ctenophora Has Implications for Metazoan Character Trait Evolution. *Curr Biol*
452 26(20):2814–2820.
453 49. Sebé-Pedrós A, et al. (2018) Early metazoan cell type diversity and the evolution of
454 multicellular gene regulation. *Nat Ecol Evol* 2(7):1176–1188.
455 50. Pang K, Martindale MQ (2008) Ctenophore whole-mount in situ hybridization. *CSH Protoc*
456 2008:db.prot5087.
457 51. Schindelin J, et al. (2012) Fiji: an open-source platform for biological-image analysis.
458 *Nature Methods* 9(7):676–682.

459 52. Kistler KE, Vosshall LB, Matthews BJ (2015) Genome engineering with CRISPR-Cas9 in
460 the mosquito Aedes aegypti. *Cell Rep* 11(1):51–60.
461 53. Xiao A, et al. (2014) CasOT: a genome-wide Cas9/gRNA off-target searching tool.
462 *Bioinformatics* 30(8):1180–1182.

463

464 **Figure Legends**

465 **Fig. 1: *MleKlf5a* and *MleKlf5b* are expressed in regions of rapid cell proliferation during**
466 **embryogenesis in *Mnemiopsis leidyi.*** Schematic depiction of tentacular axis (TA) and
467 pharyngeal axis (PA) orientation are located in panel upper right. Aboral view in **a, c, e, g, j, l,**
468 **m, o, q, s, u, w**. Lateral view, oral up, in **b, d, f, h, k, n, p, r, t, v, x**. Scale bars are 50 µm. (**a-h**)
469 25 min EdU pulse in 13 hours post fertilization (hpf) (**a-d**) and 16 hpf (**e-h**) embryos. EdU
470 incorporation is localized to two cell clusters in the apical organ (**a, e**), epithelial cells flanking
471 the developing ctene rows (bounded by dashed lines) (**b, f**), epithelial cells lining the
472 gastrovascular cavity (gvc) (**d, h**) in the developing tentacular median ridges (arrowheads), and
473 the oral (oph) and aboral (aph) regions of the pharynx (**d**). (**g, h**) Later in development, EdU
474 incorporation is found in the tentacular median ridge (arrowheads) and lateral ridges (lr) of the
475 tentacle bulbs and in both oral (oph) and aboral (aph) regions of the pharynx. (**i-x**) mRNA
476 expression patterns for *MleKlf5a* and *MleKlf5b* during embryogenesis. Maternal transcripts for
477 both *MleKlf5a* (**i, j**) and *MleKlf5b* (**k, l**) are found ubiquitously in zygotes (**i**), early cleavage
478 stages (**k**) and gastrulae (**j, l**). (**m-p**) Zygotic *MleKlf5a* and *MleKlf5b* transcripts exhibit
479 overlapping endodermal expression domains. At 9 hpf expression of *MleKlf5a* and *MleKlf5b*
480 transcripts are localized to the forming tentacular median ridges (arrowheads) and the developing
481 pharynx (oph + aph). (**q-t**) At 14 hpf *MleKlf5a* and *MleKlf5b* transcript expression is also found

482 in the apical organ (arrows) and epithelia of the newly formed gastrovascular cavity (gvc). (**u-x**)
483 At 20 hpf *MleKlf5a* and *MleKlf5b* transcripts are found in the tentacular median ridge
484 (arrowheads) and lateral ridge (lr), on either side of the apical organ floor (arrows), localized
485 towards the aboral end of the pharynx (aph), and the gastrovascular cavity epithelium (gvc).
486
487 **Fig. 2: Two independent methods used to abrogate *MleKlf5a* and *MleKlf5b* gene function.**
488 *MleKlf5a* (**a**) and *MleKlf5b* (**e**) exon-intron schematics show the location of sbMO targets (blue
489 boxes) and sgRNA targets (black triangle) used in this study. (**b,f**) Electrophoretic gels of PCR
490 products obtained using *MleKlf5a* and *MleKlf5b* sbMO RT-PCR primers (arrows in predicted
491 spliceform schematics to the right) on cDNA obtained from an individual morphant exemplar (*n*
492 = 21 morphants). 2-log DNA ladder was used for band size reference. Wildtype (wt) and mis-
493 spliced transcripts due to exon-skipping (-E) and/or intron retention (+I) were present in
494 morphants. (**c-d, g-h**) Crispant discordance plots and corresponding Sanger sequence traces.
495 sgRNA target site is underlined, Cas9 cut site is represented by dashed line and shows clearly
496 elevated sequence discordance relative to genome sequence reference and control sanger
497 sequencing. Sanger sequencing signal degradation is caused by the introduction of indels in an
498 individual crispant exemplar (*n* = 17 crispants; also see **S3b**).
499
500 **Fig. 3: *MleKlf5a* and *MleKlf5b* double gene knockdown via sbMO and *sgRNA*-Cas9 genome**
501 **editing.** (**a-p**) Live imaging showing morphology of 20 hpf cydippids. Aboral view in **a, c, e, g,**
502 **i, k, m, o**. Lateral view, oral up, in **b, d, f, h, j, l, n, p, q, r**. Schematic depiction of tentacular
503 axis (TA) and pharyngeal axis (PA) orientation are located in panel upper right. Scale bars are 50
504 µm. Hoechst (blue) marks nuclei. Mitotracker (red) preferentially marks position of ctene row

505 polster cells, one pair per embryonic quadrant. Lysotracker (yellow) preferentially stains
506 epithelial cells lining the gastrovascular cavity (gvc). Tentacular median ridges (arrowheads) are
507 positioned medially along the tentacular axis and contacted by gvc epithelial cells. The pharynx
508 (ph) is positioned centrally and joins with the gvc aborally. The apical organ (arrow) is located at
509 the aboral pole of the embryo. Un-injected wildtype embryo (**a, b**). Morphology is unaffected in
510 embryos sham injected with control morpholino (MO) (**c, d**), *sgRNA* only (**i, j**) or Cas9 protein
511 only (**k, l**). In contrast, mild phenotypes in double gene knockdown morphants (**e, f**) and double
512 gene edited crispants (**m, n**) display aberrant distributions of gvc epithelial cells (Lysotracker
513 signal), aberrant patterning of the pharynx (ph) including aboral bifurcations (**f**, **n**, **S4**, **S5**),
514 aberrant patterning of the tentacle bulb and tentacular median ridges (arrowheads), and atypical
515 apical organ (arrow) morphology. Severe phenotypes in double gene knockdown morphants (**g,**
516 **h**) and double gene edited crispants (**o, p**) are reduced in size due to lack of mesogleal ECM
517 extrusion, display collapsed pharynx with gvc junction defects, significantly reduced tentacle
518 bulbs and tentacular median ridges (arrowheads), and apical organ defects (arrow). (**q**) 25 min
519 EdU pulse in wildtype 16 hpf embryo. Strong EdU incorporation signal (orange) is found in the
520 oral (oph) and aboral (aph) regions of the developing pharynx, epithelial cells lining the
521 gastrovascular cavity (gvc), the developing tentacular median ridges (arrowheads) and lateral
522 ridges (lr) of the tentacle bulbs. (**r**) 25 min EdU pulse in 16 hpf crispant embryo. EdU
523 incorporation signal (orange) is significantly diminished in regions that also express *MleKlf5a*
524 and *MleKlf5b* (refer to **Fig. 1**) including the pharynx, gvc and tentacular median ridges. Note that
525 lr cell proliferation is not affected. (**s**) Comparison of phenotypic proportions in morphants (n =
526 45) (51% no phenotype, 29% mild phenotype, 20% severe phenotype) vs crispants (n = 16) (6%
527 no phenotype, 19% mild phenotype, 75% severe phenotype).

528

529 **Fig. 4: *MleKlf5a* and *MleKlf5b* double gene knockdown negatively affects apical organ**
530 **lithocyte production and negatively affects tentacular median ridge size.** Live images of
531 embryos at 20 hpf. Schematic depiction of tentacular axis (TA) and pharyngeal axis (PA)
532 orientation are located in panel upper right. Aboral view in **a, c, e, h, j, l**. Lateral view, oral up, in
533 **b, d, f, i, k, m**. Scale bars are 50 µm. (**a, b**) lithocytes (arrow), dome cilia (arrowhead) and apical
534 organ (ao) in wildtype embryo. (**c, d**) double gene knockdown morphant lacking lithocytes. (**e, f**)
535 double gene edited crispant lacking lithocytes. Dome cilia (arrowheads) and balancer cilia are
536 present in both morphants and crispants. (**g**) *MleKlf5a* and *MleKlf5b* double gene knockdown
537 significantly reduces lithocyte production. Box plot center lines show medians, box limit at 25th
538 and 75th percentiles, whiskers extend 1.5 times interquartile range from the 25th and 75th
539 percentiles, data points are plotted as open circles. * = two-tailed *t*-test, $t = 3.47$, $p<0.005$. ** =
540 two-tailed *t*-test, $t = 6.52$, $p<0.00001$. Wildtype ($n = 14$), morphant ($n = 33$), crispant ($n = 15$).
541 (**h, i**) Wildtype tentacular median ridge (arrowhead) and lateral ridge (lr). (**j, k**) double gene
542 knockdown morphant with dramatically reduced tentacular median ridge. (**l, m**) double gene
543 edited crispant with dramatically reduced tentacular median ridge. The tentacle bulb lateral ridge
544 remains present in both morphants and crispants. (**n**) *MleKlf5a* and *MleKlf5b* double gene
545 knockdown significantly reduces tentacular median ridge length. Box plot center lines show the
546 median, box limit at 25th and 75th percentiles, whiskers extend 1.5 times interquartile range
547 from the 25th and 75th percentiles, data points are plotted as open circles. * = two-tailed *t*-test, t
548 $= 4.01$, $p<0.0005$. ** = two-tailed *t*-test, $t = 8.32$, $p<0.00001$. Each data point represents a single
549 tentacular median ridge length, with a maximum of 2 data points (i.e., 2 tentacular median

550 ridges) from each embryo. Data value of 0 indicate the absence of a tentacular median ridge
551 and/or tentacle bulb. Wildtype (n = 28), morphant (n = 61), crispant (n = 34).
552
553 **S1: Proliferating cells in the tentacular median ridge give rise to tentacle muscle in *M.***
554 ***leidyi*.** Aboral view and schematic depiction of tentacular axis (TA) and pharyngeal axis (PA)
555 orientation are located in panel upper right. Scale bars are 50 µm. EdU pulse:chase
556 immunohistochemistry on tentacle bulbs (**a**) after 25 min pulse:0 min chase and (**b**) after 25 min
557 pulse:24 hr chase. (**a**) 25 min pulse EdU marks rapidly proliferating cells in the tentacular
558 median ridge (arrow) and lateral ridges (lr) of the tentacle bulb. (**b**) After 25 min pulse:24 hr
559 chase, EdU incorporation is primarily detected in emergent tentacle muscle cells.
560
561 **S2: Additional *MleKlf5b* and *MleKlfX* transcript expression domains.** Schematic depiction of
562 tentacular axis (TA) and pharyngeal axis (PA) orientation are located in panel upper right. Scale
563 bars are 50 µm. (**a, b**) 9 hpf and 14 hpf embryos, lateral view, oral up. Dashed lines bound
564 *MleKlf5b* ectodermal expression (magenta) in rapidly dividing cells (compare with **Fig. 1b, f**)
565 that flank developing ctene row pairs (visible as aligned columns of DAPI stained nuclei
566 bounded by *MleKlf5b* expression). (**c, d**) Magnified aboral views of *MleKlfX* expression
567 (magenta) in epithelial floor cells of the apical organ. (**c**) Initially *MleKlfX* expression is detected
568 at 16 hpf in four small clusters of cells at the boundary of each developing embryonic quadrant
569 converging in the center of the apical organ. (**d**) Expression of *MleKlfX* resolves into several cell
570 clusters by 18 hpf in both the tentacular (TA) and pharyngeal (PA) axes.
571

572 **S3: ICE analysis of Crispants.** (**a**) Sham injection has no effect on embryonic development. Bar
573 graph comparison of percentage of normal development in wildtype n = 161 (24 abnormal);
574 devitellinized but uninjected n = 217 (42 abnormal), two-tailed Fisher's exact test p = 0.2761;
575 control MO injected n = 49 (10 abnormal), two-tailed Fisher's exact test p = 0.379; Cas9 only
576 injected n = 7 (1 abnormal), two-tailed Fisher's exact test p = 1; sgRNA only injected n = 4 (1
577 abnormal), two-tailed Fisher's exact test p = 0.4851. (**b**) Distribution of ICE scores (estimate of
578 indel proportion in signal trace from genomic DNA of individual crispants) and KO scores
579 (estimate of indel proportion that result in frameshift mutation) for *MleKlf5a-sgRNA4* (n = 14)
580 and *MleKlf5b-sgRNA3* (n = 17). Cas9 cut sites were PCR amplified from genomic DNA
581 prepared from individual crispants and subsequently Sanger sequenced. Each cut site data point
582 represents Sanger trace analyses from an individual embryo. Box plot center lines show the
583 median, box limit at 25th and 75th percentiles, whiskers extend 1.5 times interquartile range
584 from the 25th and 75th percentiles, data points are plotted as open circles.
585
586 **S4: Cas9 mediated genome editing of either *MleKlf5a* or *MleKlf5b* resulted in reduced**
587 **phenotype penetrance.** Schematic depiction of tentacular axis (TA) orientation located in panel
588 upper right. Lateral view, oral up, scale bars are 50 µm. Single gene editing produced primarily
589 mild phenotypes for both *MleKlf5a* crispants (**a**) and *MleKlf5b* crispants (**b**). (**c**) Bar graph
590 comparison of distribution of mild (gray) vs severe (black) phenotypes in *MleKlf5a* crispants (n
591 = 5, 80% mild) and *MleKlf5b* crispants (n = 5, 80% mild).
592
593 **S5: Aberrant pharyngeal patterning.** Schematic depiction of tentacular axis (TA) and
594 pharyngeal axis (PA) orientation located in panel upper right. Lateral views, oral up, scale bars

595 are 50 µm. (**a, b**) 20 hpf double gene morphant embryo with bifurcated (arrow) pharynx (ph). (**c,**
596 **d**) Same individual morphant 3 days post fertilization (dph) showing persistence of pharyngeal
597 bifurcation patterning defect just anterior of the pharyngeal-gastrovascular junction resulting in a
598 deletion of the pharyngeal folds.
599
600 **S6: Schematic of cydippid tentacle bulb.** Aboral top, lateral bottom. Tentacular median ridge
601 colored light gray. Tentacular lateral ridges colored darker gray. Tentacle (not shown) is rooted
602 at the aboral medial base of the tentacle bulb. Location of measurement taken for the tentacular
603 median ridge length (refer to **Fig. 4n**) is denoted with red dashed line.
604

605 **ACKNOWLEDGEMENTS**

606 This work was supported in part by startup funds from the University of Miami College of Arts
607 and Sciences to WEB. JSP was supported by the University of Miami College of Arts and
608 Sciences. We thank Ricardo Cepeda for additional animal support.
609

610 **AUTHOR CONTRIBUTIONS**

611 WEB originally conceived the study and designed the research. JSP and WEB performed
612 experiments, collected and analyzed data, and wrote the manuscript. JSP and WEB read and
613 approved the final manuscript.
614

615 **AUTHOR INFORMATION**

616 Correspondence and requests for materials should be addressed to WEB.
617 (w.browne@miami.edu)

618

619 **Competing financial interests:** The authors declare no competing financial interests.

Figure1

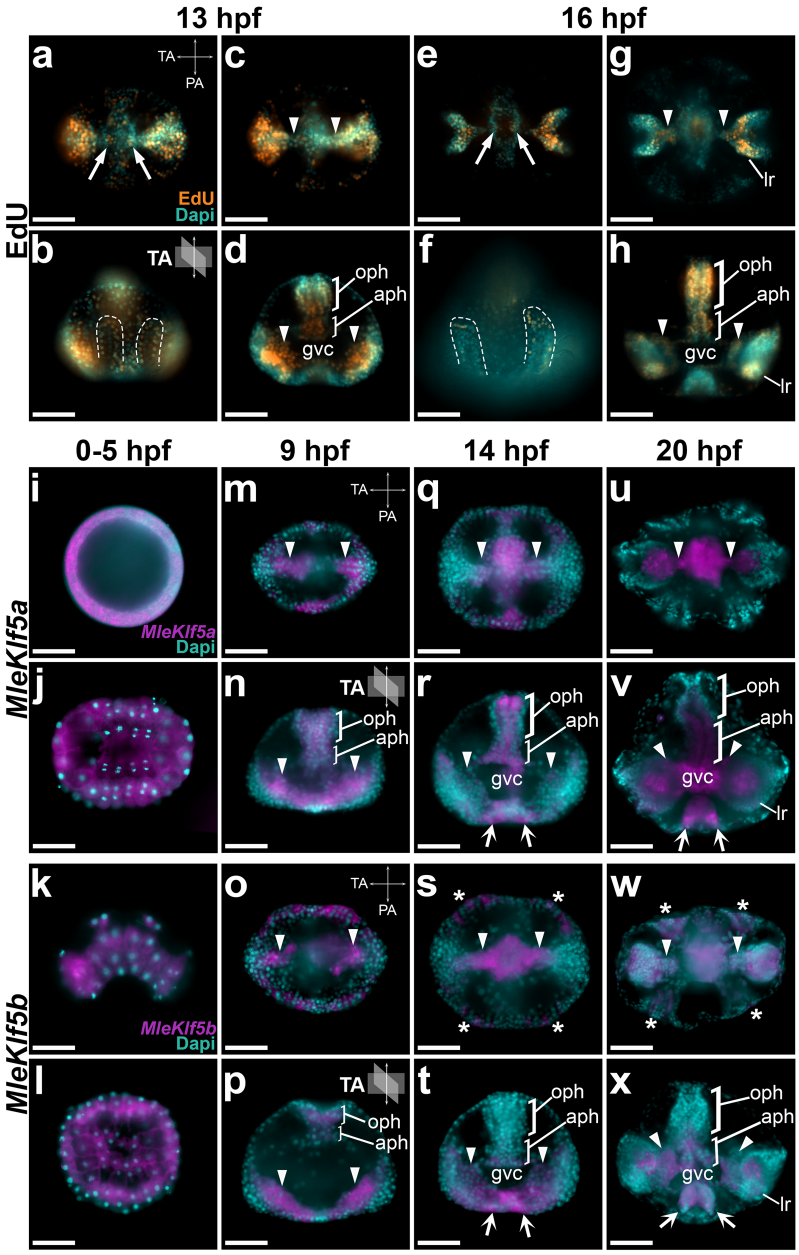

Figure 1. *MleKlf5a* and *MleKlf5b* are expressed in regions of rapid cell proliferation during embryogenesis in *Mnemiopsis leidyi.* Schematic depiction of tentacular axis (TA) and pharyngeal axis (PA) orientation are located in panel upper right. Aboral view in **a, c, e, g, j, l, m, o, q, s, u, w**. Lateral view, oral up, in **b, d, f, h, k, n, p, r, t, v, x**. Scale bars are 50 µm. **(a-h)** 25 min EdU pulse in 13 hours post fertilization (hpf) (**a-d**) and 16 hpf (**e-h**) embryos. EdU incorporation is localized to two cell clusters in the apical organ (**a, e**), epithelial cells flanking the developing ctene rows (bounded by dashed lines) (**b, f**), epithelial cells lining the gastrovascular cavity (gvc) (**d, h**) in the developing tentacular median ridges (arrowheads), and the oral (oph) and aboral (aph) regions of the pharynx (**d**). **(g, h)** Later in development, EdU incorporation is found in the tentacular median ridge (arrowheads) and lateral ridges (lr) of the tentacle bulbs and in both oral (oph) and aboral (aph) regions of the pharynx. **(i-x)** mRNA expression patterns for *MleKlf5a* and *MleKlf5b* during embryogenesis. Maternal transcripts for both *MleKlf5a* (**i, j**) and *MleKlf5b* (**k, l**) are found ubiquitously in zygotes (**i**), early cleavage stages (**k**) and gastrulae (**j, l**). **(m-p)** Zygotic *MleKlf5a* and *MleKlf5b* transcripts exhibit overlapping endodermal expression domains. At 9 hpf expression of *MleKlf5a* and *MleKlf5b* transcripts are localized to the forming tentacular median ridges (arrowheads) and the developing pharynx (oph + aph). **(q-t)** At 14 hpf *MleKlf5a* and *MleKlf5b* transcript expression is also found in the apical organ (arrows) and epithelia of the newly formed gastrovascular cavity (gvc). **(u-x)** At 20 hpf *MleKlf5a* and *MleKlf5b* transcripts are found in the tentacular median ridge (arrowheads) and lateral ridge (lr), on either side of the apical organ floor (arrows), localized towards the aboral end of the pharynx (aph), and the gastrovascular cavity epithelium (gvc).

Figure2

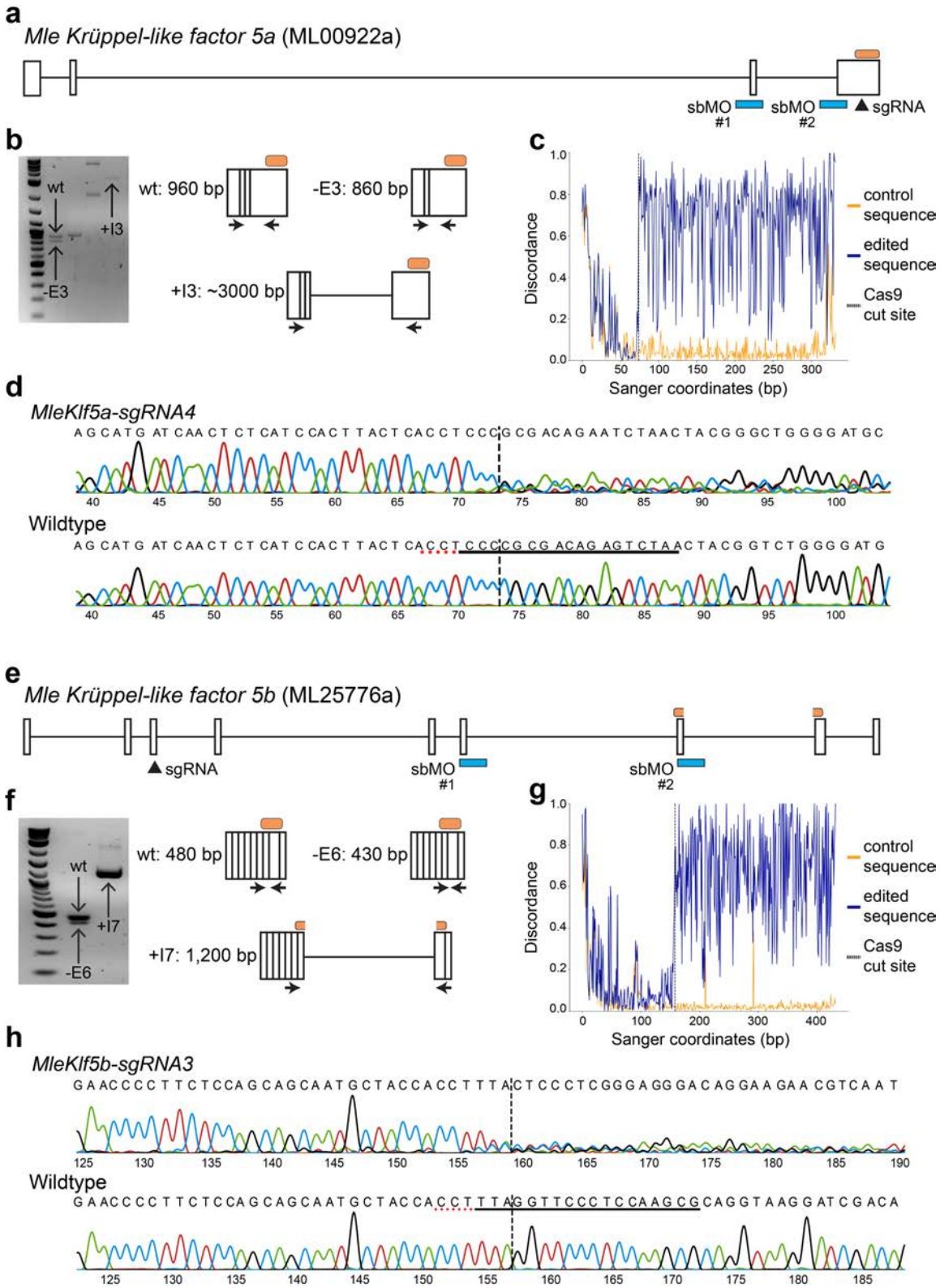

Figure 2. Two independent methods used to abrogate *MleKlf5a* and *MleKlf5b* gene function. *MleKlf5a* (**a**) and *MleKlf5b* (**e**) exon-intron schematics show the location of sbMO targets (blue boxes) and sgRNA targets (black triangle) used in this study. (**b,f**) Electrophoretic gels of PCR products obtained using *MleKlf5a* and *MleKlf5b* sbMO RT-PCR primers (arrows in predicted spliceform schematics to the right) on cDNA obtained from an individual morphant exemplar (n = 21 morphants), 2-log DNA ladder was used for band size reference. Wildtype (wt) and mis-spliced transcripts due to exon-skipping (-E) and/or intron retention (+I) were present in morphants. (**c-d, g-h**) Crispant discordance plots and corresponding Sanger sequence traces. sgRNA target site is underlined, Cas9 cut site is represented by dashed line and shows clearly elevated sequence discordance relative to genome sequence reference and control sanger sequencing. Sanger sequencing signal degradation is caused by the introduction of indels in an individual crispant exemplar (n = 17 crispants; also see **EDF3b**).

Fig3

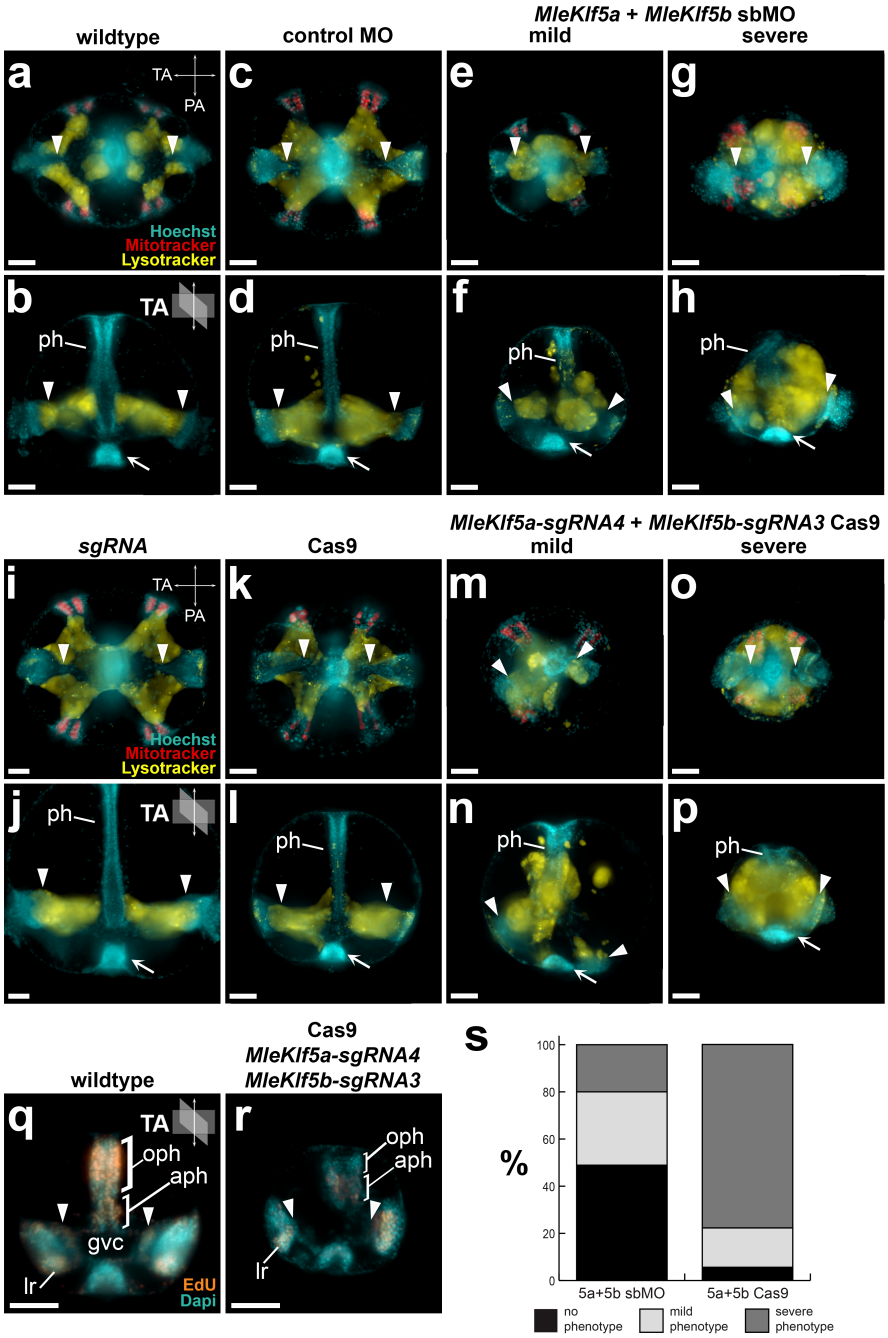

Figure 3. ***MleKlf5a* and *MleKlf5b* double gene knockdown via sbMO and *sgRNA*-Cas9 genome editing.** (**a-p**) Live imaging showing morphology of 20 hpf cydippids. Aboral view in **a, c, e, g, i, k, m, o**. Lateral view, oral up, in **b, d, f, h, j, l, n, p, q, r**. Schematic depiction of tentacular axis (TA) and pharyngeal axis (PA) orientation are located in panel upper right. Scale bars are 50 µm. Hoechst (blue) marks nuclei. Mitotracker (red) preferentially marks position of ctene row polster cells, one pair per embryonic quadrant. Lysotracker (yellow) preferentially stains epithelial cells lining the gastrovascular cavity (gvc). Tentacular median ridges (arrowheads) are positioned medially along the tentacular axis and contacted by gvc epithelial cells. The pharynx (ph) is positioned centrally and joins with the gvc aborally. The apical organ (arrow) is located at the aboral pole of the embryo. Un-injected wildtype embryo (**a, b**). Morphology is unaffected in embryos sham injected with control morpholino (MO) (**c, d**), *sgRNA* only (**i, j**) or Cas9 protein only (**k, l**). In contrast, mild phenotypes in double gene knockdown morphants (**e, f**) and double gene edited crispants (**m, n**) display aberrant distributions of gvc epithelial cells (Lysotracker signal), aberrant patterning of the pharynx (ph) including aboral bifurcations (**f**, **n**, **EDF4**, **EDF5**), aberrant patterning of the tentacle bulb and tentacular median ridges (arrowheads), and atypical apical organ (arrow) morphology. Severe phenotypes in double gene knockdown morphants (**g, h**) and double gene edited crispants (**o, p**) are reduced in size due to lack of mesogleal ECM extrusion, display collapsed pharynx with gvc junction defects, significantly reduced tentacle bulbs and tentacular median ridges (arrowheads), and apical organ defects (arrow). (**q**) 25 min EdU pulse in wildtype 16 hpf embryo. Strong EdU incorporation signal (orange) is found in the oral (oph) and aboral (aph) regions of the developing pharynx, epithelial cells lining the gastrovascular cavity (gvc), the developing tentacular median ridges (arrowheads) and lateral ridges (lr) of the tentacle bulbs. (**r**) 25 min EdU pulse in 16 hpf crispant embryo. EdU incorporation signal (orange) is significantly diminished in regions that also express *MleKlf5a* and *MleKlf5b* (refer to **Fig. 1**) including the pharynx, gvc and tentacular median ridges. Note that lr cell proliferation is not affected. (**s**) Comparison of phenotypic proportions in morphants ($n = 45$) (51% no phenotype, 29% mild phenotype, 20% severe phenotype) vs crispants ($n = 16$) (6% no phenotype, 19% mild phenotype, 75% severe phenotype).

Fig4

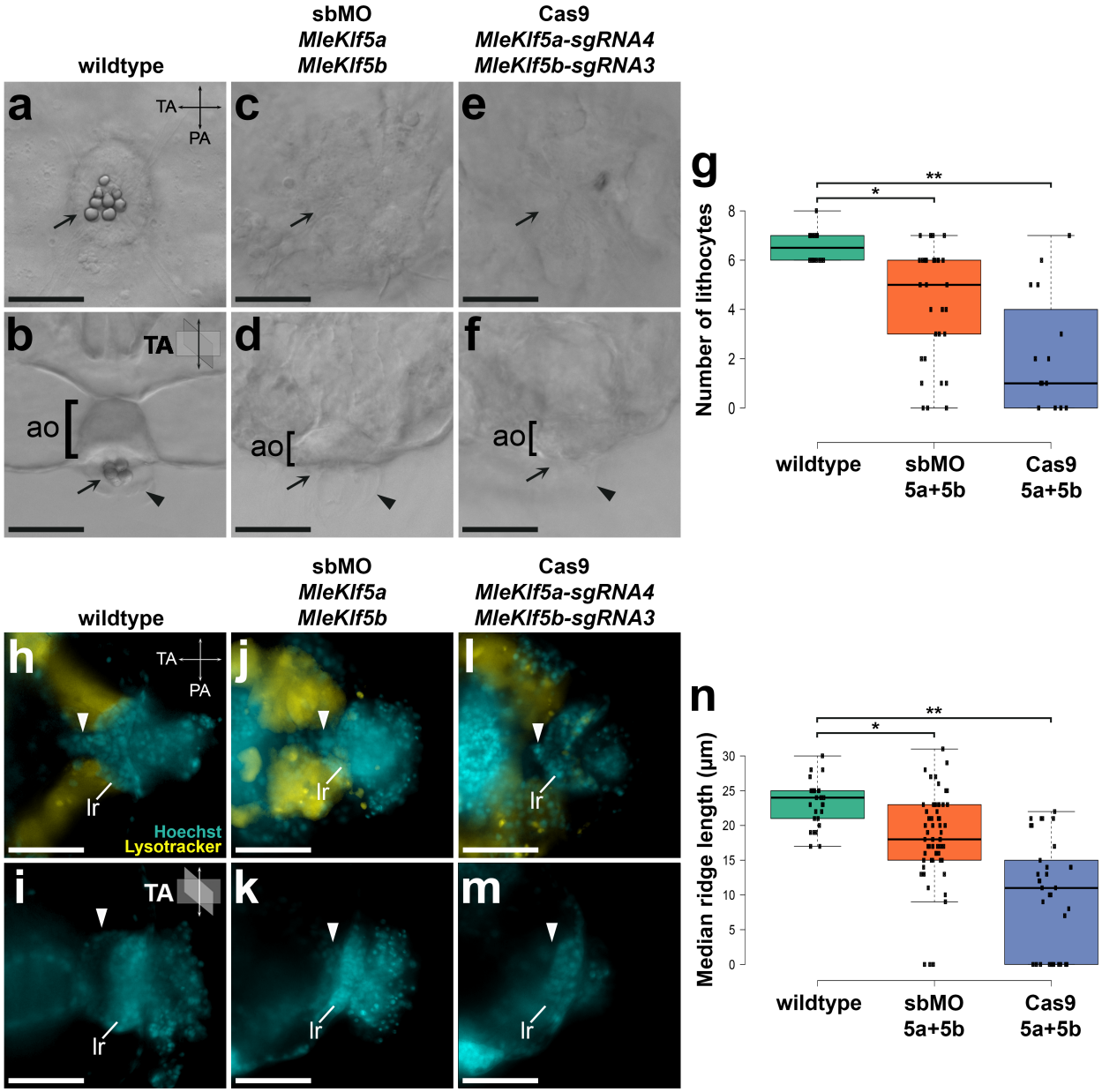

Figure 4. *MleKlf5a* and *MleKlf5b* double gene knockdown negatively affects apical organ lithocyte production and negatively affects tentacular median ridge size. Live images of embryos at 20 hpf. Schematic depiction of tentacular axis (TA) and pharyngeal axis (PA) orientation are located in panel upper right. Aboral view in **a, c, e, h, j, l**. Lateral view, oral up, in **b, d, f, i, k, m**. Scale bars are 50 µm. (**a, b**) lithocytes (arrow), dome cilia (arrowhead) and apical organ (ao) in wildtype embryo. (**c, d**) double gene knockdown morphant lacking lithocytes. (**e, f**) double gene edited crispant lacking lithocytes. Dome cilia (arrowheads) and balancer cilia are present in both morphants and crispants. (**g**) *MleKlf5a* and *MleKlf5b* double gene knockdown significantly reduces lithocyte production. Box plot center lines show medians, box limit at 25th and 75th percentiles, whiskers extend 1.5 times interquartile range from the 25th and 75th percentiles, data points are plotted as open circles. * = two-tailed *t*-test, = 3.47, <0.005. ** = two-tailed *t*-test, = 6.52, <0.00001. Wildtype (n = 14), morphant (n = 33), crispant (n = 15). (**h, i**) Wildtype tentacular median ridge (arrowhead) and lateral ridge (lr). (**j, k**) double gene knockdown morphant with dramatically reduced tentacular median ridge. (**l, m**) double gene edited crispant with dramatically reduced tentacular median ridge. The tentacle bulb lateral ridge remains present in both morphants and crispants. (**n**) *MleKlf5a* and *MleKlf5b* double gene knockdown significantly reduces tentacular median ridge length. Box plot center lines show the median, box limit at 25th and 75th percentiles, whiskers extend 1.5 times interquartile range from the 25th and 75th percentiles, data points are plotted as open circles. * = two-tailed *t*-test, = 4.01, <0.0005. ** = two-tailed *t*-test, = 8.32, <0.00001. Each data point represents a single tentacular median ridge length, with a maximum of 2 data points (i.e., 2 tentacular median ridges) from each embryo. Data value of 0 indicate the absence of a tentacular median ridge and/or tentacle bulb. Wildtype (n = 28), morphant (n = 61), crispant (n = 34).

Table1

Table 1 | Primers and Oligonucleotides used in this study. All sequences are oriented 5'-3'. Blue nucleotide sequences correspond to T7 promoter. Black bold italicized nucleotide sequences correspond to genomic *MleKlf* targets and include addition of two 5' *G* residues to aid T7 polymerase binding. Red nucleotide sequences denote region of complementary between templated primers and Universal tracrRNA primer, which are annealed to the form the sgRNA transcription template.

Name	Use	Forward	Reverse
MleKlf5a	ISH probe	ATGAGTGCTATGACATG	AAACGTGTTCAAATGCCTCTT
MleKlf5b	ISH probe	ATGGACGTTTCCACGC	AGACGAGCTAGGGGGAACG
MleKlfX	ISH probe	GGCAGTTTAGTTCGATCGG	TGCAGTGAGTGGTAGGTT
MleKlf5a sbMO#1	sbMO	TCTCGTGTCTGAAACAATTTTAAGT	n/a
MleKlf5a sbMO#2	sbMO	GTCTACCACCTGCAAGATTTTAAGT	n/a
MleKlf5b sbMO#1	sbMO	CAGTTGATTTCTCACCTGCCAAGAA	n/a
MleKlf5b sbMO#2	sbMO	CAAACAGACTTACCTTCAAATGTGA	n/a
Standard Control	sbMO	CCTCTTACCTCAGTTACAATTTATA	n/a
MleKlf5a sbMO RT-PCR	sbMO validation	CCCTTGTAAACTTGAGCA	TCTTCGTGTAAACCTTCG
MleKlf5b sbMO RT-PCR	sbMO validation	GACAAGTTCCAAAGACTAAC	TACAGTAGATGAGGAGGTTT
Universal tracrRNA	sgRNA synthesis	AAAAGCACCGACTCGGTGCCACTTTTTCAAGTTGATAACGGACTAGCCTTATTTTAACTTGCTATTTCTAGCTCTAAAAC	n/a
sgRNA template	sgRNA synthesis	GAAATTAATACGACTCACTATA**GG[N_{XX}]**GTTTTAGAGCTAGAAATAGC	n/a
MleKlf5a-gRNA1	sgRNA synthesis	AGCAACGGGTCCGTCCGT	n/a

Table1

MleKlf5a-gRNA2	sgRNA synthesis	TTGAGGGACGCGGGAGCAA	n/a
MleKlf5a-gRNA3	sgRNA synthesis	ACGGAGGGAATCGGCGAT	n/a
MleKlf5a-gRNA4	sgRNA synthesis	TTAGACTCTGTCGCGGGG	n/a
MleKlf5b-gRNA1	sgRNA synthesis	TGGTGATATACCAGGCG	n/a
MleKlf5b-gRNA2	sgRNA synthesis	ATCTTTCACGCTTAGGGGC	n/a
MleKlf5b-gRNA3	sgRNA synthesis	CGCTTGGAGGGAACCTAA	n/a
MleKlf5b-gRNA4	sgRNA synthesis	CTGAAACACCGGTCGCAG	n/a
MleKlf5a-sgRNA4 sequencing	sgRNA/Cas9 cut site validation	AAGACGTCCGATATTCTCTC	GGTGATCACTCCTACTGAAA
MleKlf5b-sgRNA3 sequencing	sgRNA/Cas9 cut site validation	GGTGTTCATACCTAGACGAT	TGTGTCTGTGTATAGTCGAG

Table 2 | Off-target CRISPR/Cas9 loci with mismatches to either *MleKlf5a* or *MleKl5b* target sequence and primers used for Sanger sequencing. All sequences are oriented 5'-3'.

Locus ID	# Mismatches	Forward	Reverse
ML090223a	4 (*MleKlf5a-sgRNA4)*	AAATTGTTTGTGTTCACACT	AGTTTTCTTTGTTTTCAGGG
ML021138a	5 (*MleKlf5a-sgRNA4)*	CAGCTTCATTGTAAAGAGTC	TTAGTTCTTATGTTTTCGCG
ML200217a	5 (*MleKlf5b-sgRNA3)*	GGATACTAGTTCCATAGCAG	CTCCTTGTTGATATTCTGGA
ML00363a	6 (*MleKlf5b-sgRNA3)*	TATGATTCTTGTTACCAGGG	ACATACGTCATCCTATTAGC
ML02979a	7 (*MleKlf5b-sgRNA3)*	CTGCATGATTACAAAGGTTT	ATGCTAAGAAGGATGCAATA

S1

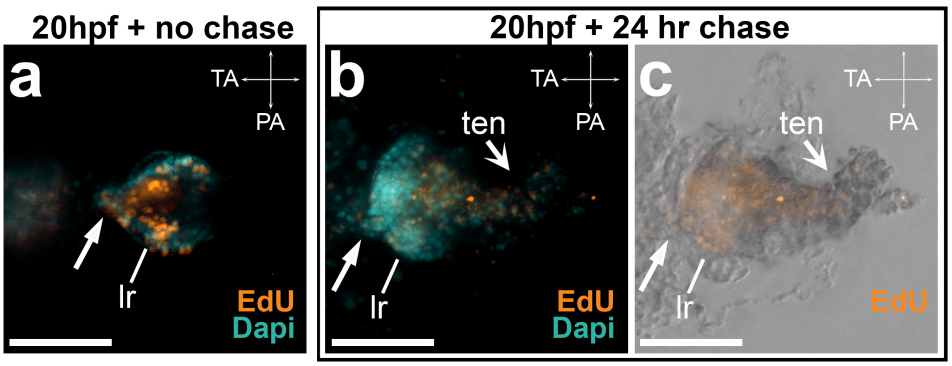

S1. Proliferating cells in the tentacular median ridge give rise to tentacle muscle in *M. leidyi*. Aboral view and schematic depiction of tentacular axis (TA) and pharyngeal axis (PA) orientation are located in panel upper right. Scale bars are 50 µm. EdU pulse:chase immunohistochemistry on tentacle bulbs (**a**) after 25 min pulse:0 min chase and (**b**) after 25 min pulse:24 hr chase. (**a**) 25 min pulse EdU marks rapidly proliferating cells in the tentacular median ridge (arrow) and lateral ridges (lr) of the tentacle bulb. (**b**) After 25 min pulse:24 hr chase, EdU incorporation is primarily detected in emergent tentacle muscle cells.

S2

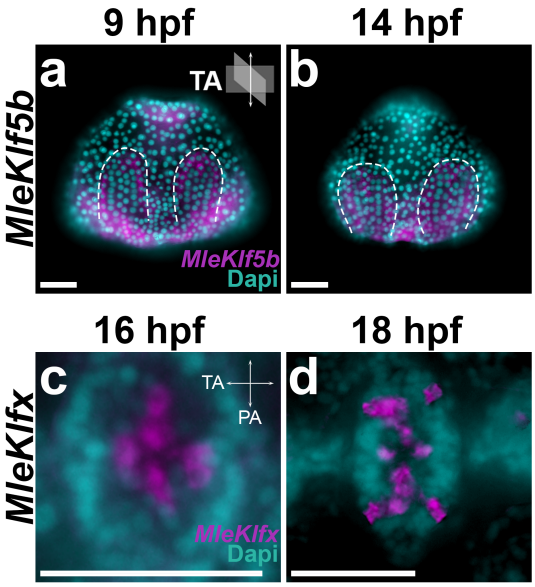

S2. Additional *MleKlf5b* and *MleKlfX* transcript expression domains. Schematic depiction of tentacular axis (TA) and pharyngeal axis (PA) orientation are located in panel upper right. Scale bars are 50 µm. (**a, b**) 9 hpf and 14 hpf embryos, lateral view, oral up. Dashed lines bound *MleKlf5b* ectodermal expression (magenta) in rapidly dividing cells (compare with **Fig. 1b, f**) that flank developing ctene row pairs (visible as aligned columns of DAPI stained nuclei bounded by *MleKlf5b* expression). (**c, d**) Magnified aboral views of *MleKlfX* expression (magenta) in epithelial floor cells of the apical organ. (**c**) Initially *MleKlfX* expression is detected at 16 hpf in four small clusters of cells at the boundary of each developing embryonic quadrant converging in the center of the apical organ. (**d**) Expression of *MleKlfX* resolves into several cell clusters by 18 hpf in both the tentacular (TA) and pharyngeal (PA) axes.

S3

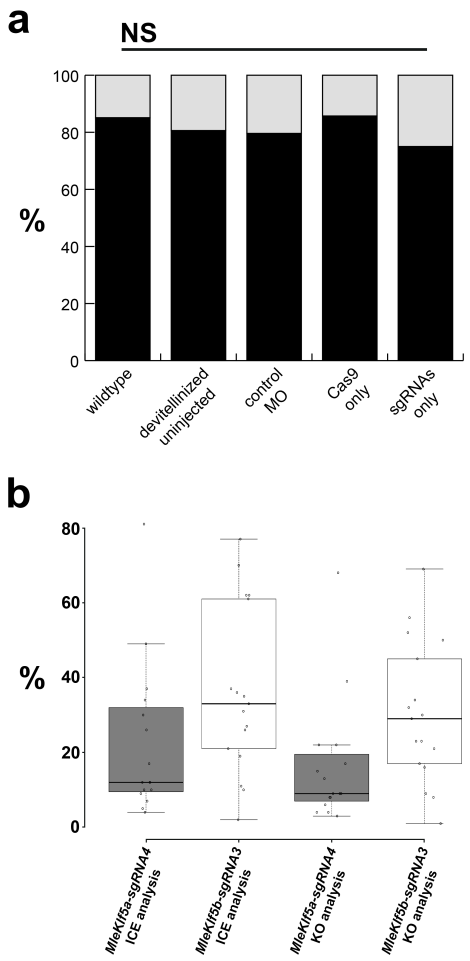

S3. ICE analysis of Crispants. (**a**) Sham injection has no effect on embryonic development. Bar graph comparison of percentage of normal development in wildtype $n = 161$ (24 abnormal); devitellinized but uninjected $n = 217$ (42 abnormal), two-tailed Fisher's exact test P=0.2761; control MO injected $n = 49$ (10 abnormal), two-tailed Fisher's exact test P=0.379; Cas9 only injected $n = 7$ (1 abnormal), two-tailed Fisher's exact test P=1; sgRNA only injected $n = 4$ (1 abnormal), two-tailed Fisher's exact test P=0.4851. (**b**) Distribution of ICE scores (estimate of indel proportion in signal trace from genomic DNA of individual crispants) and KO scores (estimate of indel proportion that result in frameshift mutation) for *MleKlf5a-sgRNA4* ($n = 14$) and *MleKlf5b-sgRNA3* ($n = 17$). Cas9 cut sites were PCR amplified from genomic DNA prepared from individual crispants and subsequently Sanger sequenced. Each cut site data point represents Sanger trace analyses from an individual embryo. Box plot center lines show the median, box limit at 25th and 75th percentiles, whiskers extend 1.5 times interquartile range from the 25th and 75th percentiles, data points are plotted as open circles.

S4

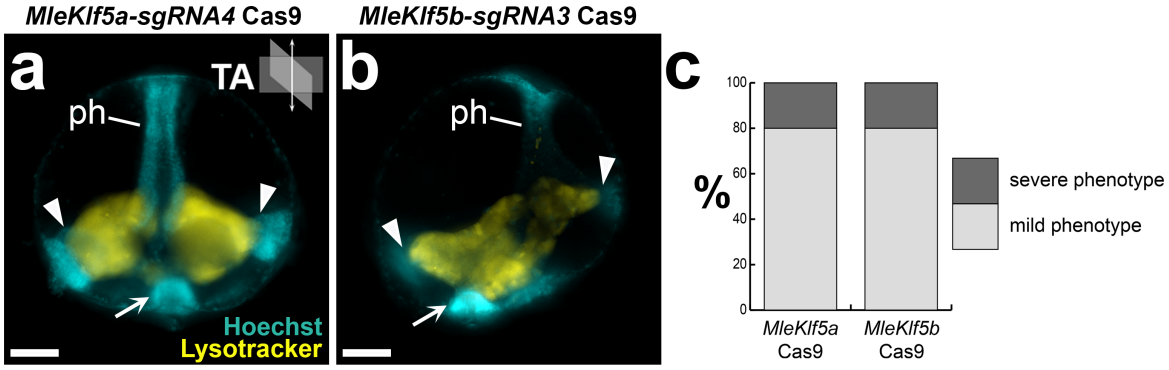

S4. Cas9 mediated genome editing of either *MleKlf5a* or *MleKlf5b* resulted in reduced phenotype penetrance. Schematic depiction of tentacular axis (TA) orientation located in panel upper right. Lateral view, oral up, scale bars are 50 µm. Single gene editing produced primarily mild phenotypes for both *MleKlf5a* crispants (**a**) and *MleKlf5b* crispants (**b**). (**c**) Bar graph comparison of distribution of mild (gray) vs severe (black) phenotypes in *MleKlf5a* crispants ($n = 5$, 80% mild) and *MleKlf5b* crispants ($n = 5$, 80% mild).

S5

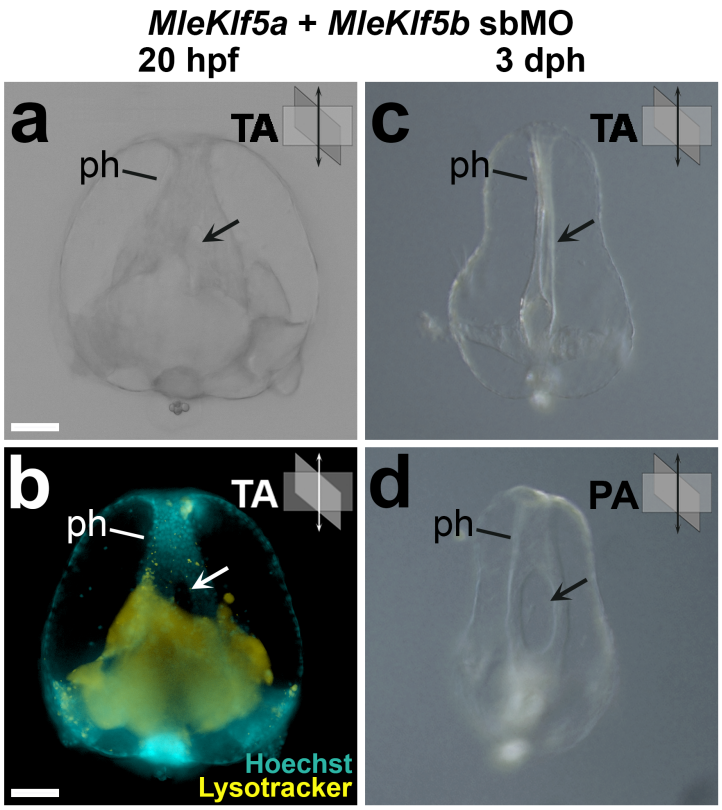

S5. Aberrant pharyngeal patterning. Schematic depiction of tentacular axis (TA) and pharyngeal axis (PA) orientation located in panel upper right. Lateral views, oral up, scale bars are 50 µm. (**a, b**) 20 hpf double gene morphant embryo with bifurcated (arrow) pharynx (ph). (**c, d**) Same individual morphant 3 days post fertilization (dph) showing persistence of pharyngeal bifurcation patterning defect just anterior of the pharyngeal-gastrovascular junction resulting in a deletion of the pharyngeal folds.

S6

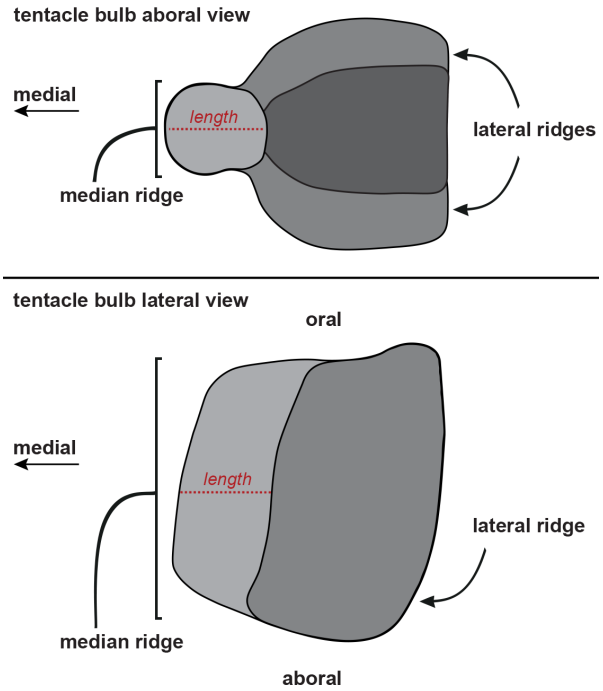

S6. Cydippid tentacle bulb schematic. Aboral top, lateral bottom. Tentacular median ridge colored light gray. Tentacular lateral ridges colored darker gray. Tentacle (not shown) is rooted at the aboral medial base of the tentacle bulb. Location of measurement taken for the tentacular median ridge length (refer to **Fig. 4n**) is denoted with red dashed line.